Feature Knowledge Based Fault Detection of Induction Motors Through the Analysis of Stator Current Data

Ting Yang, Haibo Pen, Zhaoxia Wang, *Member, IEEE*, and Che Sau Chang

***Abstract*— The fault detection of electrical or mechanical anomalies in induction motors has been a challenging problem for researchers over decades to ensure the safety and economic operations of industrial processes. To address this issue, this paper studies the stator current data obtained from inverter-fed laboratory induction motors and investigates the unique signatures of the healthy and faulty motors with the aim of developing knowledge based fault detection method for performing online detection of motor fault problems, such as broken-rotor-bar and bearing faults. Stator current data collected from induction motors were analyzed by leveraging fast Fourier transform (FFT), and the FFT results were further analyzed by the independent component analysis (ICA) method to obtain independent components and signature features that are referred to as FFT-ICA features of stator currents. The resulting FFT-ICA features contain rich information on the signatures of the healthy and faulty motors, which are further analyzed to build a feature knowledge database for online fault detection. Through case studies, this paper demonstrated the high accuracy, simplicity, and robustness of the proposed fault detection scheme for fault detection of induction motors. In addition, with the integration of the feature knowledge database, prior knowledge of the motor parameters, such as rotor speed and per-unit slip, which are needed by the other motor current signature analysis (MCSA) methods, is not required for the proposed method, which makes it more efficient compared with the other MCSA methods.**

***Index Terms*— Data analysis, fast Fourier transform (FFT), fault detection, feature knowledge database, independent component analysis (ICA), induction motors, stator current analysis.**

I. Introduction

EARLY detection of electrical or mechanical anomalies in induction motors is important for ensuring safe and economic operation of industrial processes [1]–[7]. There has been a significant amount of research in this area, including vibration analysis [8]–[11] and motor-current analysis or motor current signature analysis (MCSA) [5], [6], [12]–[15]. Even though vibration and thermal monitoring methods have been employed for decades, most of the previous research on online monitoring or periodic inspections of induction motors are based on stator-current analysis, which are well known for providing nonintrusive continuous monitoring [16]–[18].

Broken-rotor-bar and bearing faults are two main fault types in induction motors [5], [6], [19], [20]. Therefore, this paper uses these two types of faults as case studies to investigate fault detection of induction motors.

Since the stator current waveform data (which are also current signal data) collected from faulty motors are essentially different from those collected from normal motors, stator-current monitoring is viewed as an important fault detection method that does not require special access to a motor [5], [6], [17]. Most research studies on this method involve decomposing and analyzing stator currents using various algorithms such as Fourier analysis, linear discriminant analysis, wavelets, neural networks, and other statistical analysis methods to decompose and analyze stator current waveforms [16], [21]–[25]. An improved rotor fault detection algorithm that uses relative harmonic indexes as a new fault indicator has also been proposed [26] along with a statistical method to analyze the spectral data [27]. Following these, smart sensors that implement methodology based on multilayer feedforward networks (MFNs) have been used to detect fault of induction motors [28], [29]. These methods mainly relate to only one type of fault, such as bearing defects or rotor faults including broken-rotor-bars, mechanical unbalance, misalignment and voltage unbalance. Different from those methods, the scheme in this paper can detect all kinds of fault types contained in the feature knowledge database. In addition to using stator-current monitoring, there are some methods to detect fault of induction motors, for example, a two-fold method that combines the analysis of currents and the analysis of infrared data to detect electromechanical failures in induction motors [30]. However, many of these algorithms are influenced by factors arising from different inverter frequencies, measurement noise, and fault conditions, some of which may lead to erroneous fault detection [31], [32].

Independent component analysis (ICA) is a powerful computational algorithm that automatically divides a multivariate signal into additive subcomponents by exploiting the mutual statistical independence of non-Gaussian source signals [33]–[37]. It is a blind source separation process

Manuscript received June 18, 2015; revised September 7, 2015; accepted September 11, 2015. Date of publication January 5, 2016; date of current version February 5, 2016. This work was supported in part by the National Program of International Science and Technology Cooperation under Grant 2013DFA11040 and in part by the National Natural Science Foundation of China under Grant 61571324 and Grant 61172014. The Associate Editor coordinating the review process was Dr. Edoardo Fiorucci. *(Ting Yang and Zhaoxia Wang equally contributed to this work.)*

T. Yang and H. Pen are with the Key Laboratory of Smart Grid, Ministry of Education, Tianjin University, Tianjin 300072, China (e-mail: yangting@tju.edu.cn).

Z. Wang is with the Institute of High Performance Computing, Agency for Science, Technology and Research, Singapore 138632, and also an adjunct professor of Tianjin University, Tianjin 300072, China (e-mail: wangz@ihpc.a-star.edu.sg).

C. S. Chang is with the Department of Electrical and Computer Engineering, National University of Singapore, Singapore 117576.

Color versions of one or more of the figures in this paper are available online at http://ieeexplore.ieee.org.

Digital Object Identifier 10.1109/TIM.2015.2498978

and has many practical applications such as those in signal processing [37]. The ICA is capable of capturing the essential structure of data in many applications, including feature extraction and signal separation, because of its property of extracting statistically independent components.

The ICA has been used for studies on fault detection in induction motors [5], [6], [35]. Widodo *et al.* [35] applied the ICA method and employed support vector machines for fault diagnosis of induction motors using vibration signals collected at the vertical, horizontal, and axial positions and current signals in three phases. A total of 78 features were extracted in the time domain for deriving ten feature parameters. Three other parameters were separately extracted from the current signals [35].

In contrast to [35], Wang and Chang [5], Wang *et al.* [6], and Chua *et al.* [15] have investigated time-domain, frequency-domain, and hybrid algorithms, respectively, and exploited the relative strengths of frequency-domain methods as well as time-domain methods [5], [6], [15]. Compared with the 78 features mentioned by Widodo *et al.* [35], less than five features were needed to detect different faults under fixed supply frequency situations [5], [6], [15]. In the previous efforts of this research [5], [6], it was discovered that both healthy and faulty motors exhibited unique frequency signatures in the frequency-domain analysis compared to the time-domain analysis. As frequency-domain signatures contain rich information, only a few features are needed to be extracted from a moderate volume of signals for detecting consistent fault detection on induction motors [5] and no prior knowledge of the motor parameters is required for obtaining the signature features [6].

The contribution of this paper is to propose a novel scheme for fault detection such as broken-rotor-bar and bearing faults. The scheme is based on building a feature knowledge database by analyzing the unique signature features found in stator current data that can be collected from healthy and faulty motors, and both fast Fourier transform (FFT) and ICA analysis are leveraged to obtain the features. The similarity principle is then applied to identify the fault type by comparing the feature of the online detected stator current data with that of the feature knowledge database. Furthermore, the proposed scheme can improve the efficiency of online fault detection at each inverter frequency and under each load level after finishing the offline training. The novelty of this paper is that it proposes a new method which makes use of a newly created healthy and faulty feature knowledge database for online fault detection of induction motors.

In addition, for simplicity of implementation, the magnitude of the stator current frequency components as well as the frequency characteristics of healthy or faulty motors [17], [23] are both leveraged in this scheme, which greatly enhances the efficiency of fault detection of induction motors for online applications.

This paper is divided into six sections. Section II reviews the MCSA methods and presents the challenges faced by them. Section III reviews the previous time-domain algorithm and highlights the problems experienced by it at different inverter frequencies. Section IV presents the details of the proposed scheme, which includes the layout of the proposed scheme, the data collections and preparations for building the feature knowledge database, theoretical analysis of the proposed method, formulation of the proposed feature knowledge based scheme, and the development of feature knowledge database. Section V presents the simulation results and performance of the proposed scheme for the case study. Section VI concludes this paper and presents possible future work.

II. Review of Motor Current Signature Analysis Methods

A. Fault Signatures

Among the many techniques developed for MCSA [5], [6], [17], [23], FFT is the most widely used tool with the discrete Fourier transform being more efficient. FFT decomposes a time domain into components of different frequencies. Motor stator current acts as an excellent transducer for detecting faults in motors. During operation, many harmonics may be present in motor current signals. Thus, frequency spectrum shows many peaks, including the inverter (fundamental) frequency and its harmonics. This is known as the motor current signatures, which are different between faulty and healthy motors, because different electrical and mechanical faults generate different signatures.

1) Signatures of Broken-Rotor-Bars: A broken-rotor-bar can be considered as some form of rotor asymmetry that causes unbalanced currents, decreased average torque, and increased torque pulsations [17]. One significant challenge in the broken-rotor-bar detection is to distinguish its respective sidebands especially under low-slip operation. Monitoring the sidebands f_b around the fundamental harmonic is a widely used approach for diagnosing broken-rotor-bars in induction motors in the following [17]:

$$f_b = f_s(1 \pm 2ks), \quad k = 1, 2, 3, \ldots \tag{1}$$

where f_s is the inverter frequency and s is the per-unit slip.

2) Signatures of Bearing Faults: Bearing faults take the form of outer-race, inner-race, ball or cage defects, which are the main causes of machine vibrations [5], [6]. The relationship of bearing vibrations to the stator-current spectra can be determined by considering the respective air-gap eccentricity, which produces anomalies in air-gap flux density. Vibrations due to bearing faults change the air-gap symmetry and machine inductances like eccentricity faults. Machine inductance variations are reflected in the stator current in terms of current harmonics, which provide an indicator of bearing faults associated with mechanical oscillations in the air gap. Bearing fault current harmonic frequencies are expressed as [5], [6]

$$f_{\text{bearing}} = |f_s \pm m f_v| \tag{2}$$

where f_s is the inverter or fundamental frequency, $m = 1, 2, 3, \ldots$ is the harmonic indexes, and f_v can be either the inner race defect frequency f_i or the outer race defect frequency f_o

$$f_{i,o} = \frac{n}{2} f_r \left[1 \pm \frac{\text{bd}}{\text{pd}} \cos\alpha\right] \tag{3}$$

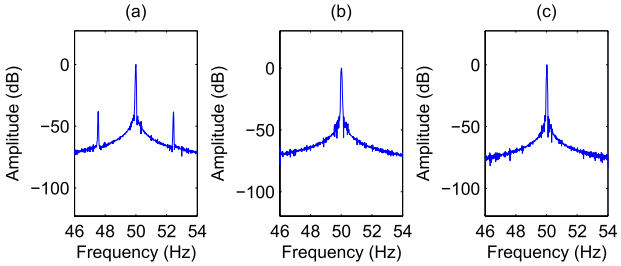

Fig. 1. Broken-rotor-bar frequency components compared with that of healthy motor under fixed-frequency supply. (a) Motor with broken-rotor-bar fault tested under full load. (b) Motor with broken-rotor-bar fault tested under no load. (c) Healthy motor.

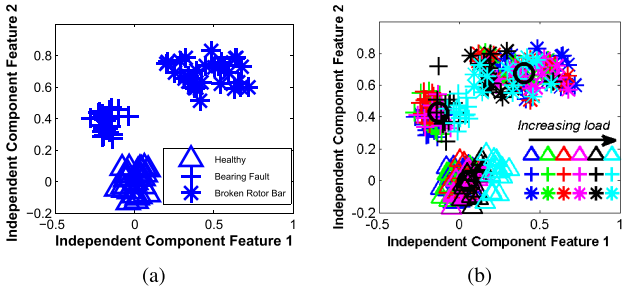

Fig. 2. Healthy and fault features of the current signals collected under fixed frequency. (a) No load. (b) With load [from no load (load level 0) to load level 5] [5], [6], [15]. Δ's—healthy. +'s—bearing fault. ∗'s—broken-rotor-bar. Blue Δ's, +'s, and ∗'s—no load. Green Δ's, +'s, and ∗'s—load level 1. Red Δ's, +'s, and ∗'s—load level 2. Pink Δ's, +'s, and ∗'s—load level 3. Black Δ's, +'s, and ∗'s—load level 4. Cyan Δ's, +'s, and ∗'s–load level 5.

where

- n number of bearing balls;
- f_r mechanical rotor speed in hertz;
- bd ball diameter;
- pd bearing pitch diameter;
- α contact angle of the balls on the races.

Further information about the bearing faults can be found in [5] and [6]. Information about the bearing construction is required to calculate the exact characteristic frequencies in (3).

B. Challenges for Classifying Healthy and Faulty Motors

1) Broken-Rotor-Bars: Accurate values of the inverter frequency and measured motor speed are required in (1) for calculating the broken-rotor-bar frequency. Fig. 1(a)–(c) shows the frequency components of the stator current from the motor with broken-rotor-bars and the healthy motor under fix-frequency supply at full load and no load. Sidebands of the broken-rotor-bars around the fundamental frequency can be explicitly observed under full load.

Challenges: It is difficult to separate a broken-rotor-bar motor under no load, as shown in Fig. 1(b) from a healthy motor, as shown in Fig. 1(c). Moreover, the broken-rotor-bar fault signatures (sidebands) depend on the inverter frequency and slip, as shown in (1). In addition, Fig. 1 shows the difficulty in distinguishing the sidebands under low load due to diminishing slips, which compounds the difficulty against using sideband as a robust means of detecting rotor bar faults under wide ranges of load and inverter frequency.

2) Bearing Faults: The inverter frequency, measured motor speed, and physical parameters of the bearing are required in (2) and (3) to calculate the bearing fault frequency. Another parameter required in (2) is the harmonic number m, which is not readily available. By applying the frequency auto search algorithm [32], the estimated bearing fault signatures f_{bearing} can be obtained. The bearing fault signature frequencies increase with the inverter frequency. The bearing fault frequency signatures are located in higher frequency band compared with the fault signatures of broken-rotor-bars [5], [6].

Challenges: Bearing faults produce harmonics in high-frequency bands, which may be close to or coincide with certain noise frequencies [5], [6]. The amplitude of some bearing fault signature frequency can be uncertain and diminishing due to noise or baseline drifting [5], [6]. These can add further problems for the detection of bearing faults if the bearing parameters are not known. Uncertain harmonics of bearing faults and other parameters, which are motor and/ or operation specific, also pose additional problems. Therefore, it is especially hard to diagnose bearing defect under changing inverter frequency.

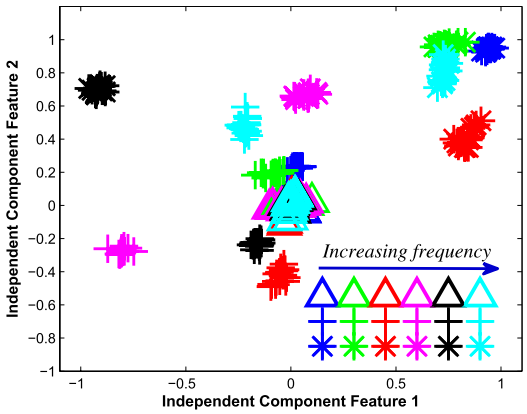

Fig. 3. Time-domain healthy and fault features of the current signals obtained using the inverter at variable frequencies. Δ's—healthy. +'s—bearing fault. ∗'s—broken-rotor-bar. Blue Δ's, +'s, and ∗'s–20 Hz. Green Δ's, +'s, and ∗'s—25 Hz. Red Δ's, +'s, and ∗'s—37.5 Hz. Pink Δ's, +'s, and ∗'s—43.5 Hz. Black Δ's, +'s, and ∗'s—50 Hz. Cyan Δ's, +'s, and ∗'s—55 Hz.

III. Review on the Previous Time-Domain Algorithm and Its Problems at Variable Frequencies

Wang and Chang [5], Wang *et al.* [6], and Chua *et al.* [15] have employed the ICA algorithm for extracting fault signatures in the time domain on measured motor stator current at a fixed frequency. A fuzzy neural network (FNN) or a fuzzy system (FS) has also been developed in [15] to classify the extracted ICA features. After learning, the FNN performs robust detection of motors having broken-rotor-bar and bearing faults supplied from fixed frequency at no load [Fig. 2(a)] and five load levels [Fig. 2(b)]. The FS is subsequently applied to the same motors supplied at different inverter frequencies with lesser performance as in the following observations [15] (Fig. 3).

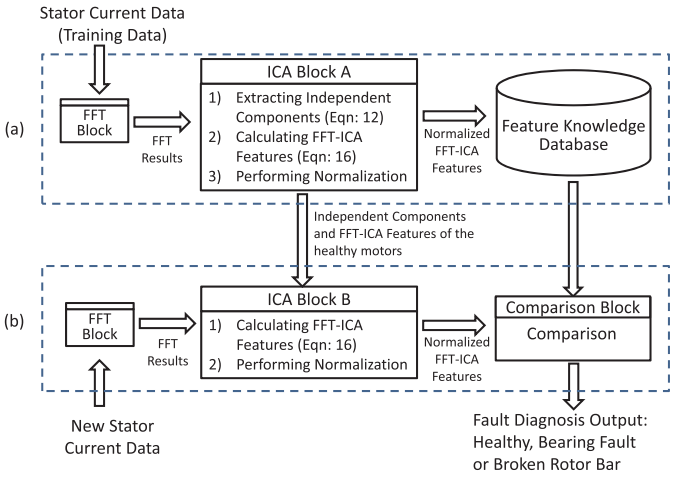

Fig. 4. Layout of the proposed feature knowledge based fault detection scheme. (a) Creation of healthy and faulty feature knowledge database. (b) Fault detection on new stator current signal data.

1) *Motors Fed From Each Fixed Inverter Frequency:* The time-domain ICA algorithm correctly classifies the two faulty signals from the healthy signals.
2) *Motors Fed From Each Different Inverter Frequency:* Drifting of the two faulty clusters is, however, clearly noteable, although the healthy cluster appears relatively stationary.

It is obvious from the above item 2) that the time-domain algorithm needs to be improved for providing robust online induction motor fault detection at variable frequencies.

IV. Proposed Feature Knowledge Based Fault Detection Scheme for Induction Motors

As mentioned in Sections II and III, the proposed method should resolve the challenges and limitations faced by the existing methods. It should have the ability to automatically perform fault detection without requiring much knowledge on induction motors in order to prove its effectiveness in meeting the target of performing consistent fault detection at different inverter frequencies. Therefore, a fault detection scheme is proposed in this paper to resolve the challenges and problems. The details on the proposed scheme will be discussed in the following sections.

A. Layout of the Proposed Scheme

The layout of the proposed scheme for online induction motor fault detection is shown in Fig. 4. It includes two computational modules: 1) creation of a feature knowledge database and 2) fault detection through the analysis of new or incoming stator current data.

As shown in Fig. 4(a), the first module builds a feature knowledge database using a collection of measured stator current data. Stator current data from nonfaulty and faulty motors are converted from time domains into frequency domains using the FFT technique in the FFT block. In ICA Block A, independent components were extracted by applying the ICA to the FFT results, and FFT-ICA features were also calculated in ICA Block A. The FFT-ICA features were then normalized by using healthy motors as benchmarks to form a feature knowledge database.

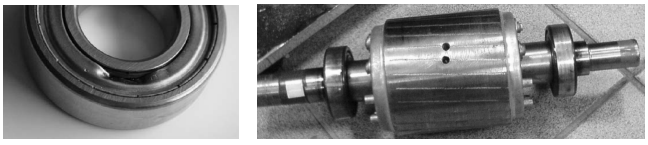

(a) (b)

Fig. 5. Fault motors. (a) Denting the seal of the bearing to simulate bearing fault. (b) Two holes are drilled on the rotor bar to simulate broken-rotor-bar fault [5], [6].

Fig. 4(b) shows the second module that performs fault diagnosis on each new stator current data. The results of the FFT and ICA Block B were used to obtain the FFT-ICA features of the new current data. Different from the ICA Block A in the first module [Fig. 4(a)], the FFT results are directly used to obtain the FFT-ICA features in ICA Block B using the independent components which are obtained in ICA Block A using the training data. The FFT-ICA features from the new current data were also normalized in ICA Block B using the FFT-ICA features of healthy motors obtained in ICA Block A. In the comparison block of Fig. 4(b), the normalized FFT-ICA features are then compared with the feature knowledge database to arrive at the fault diagnosis decision.

In the proposed scheme, the feature knowledge database for describing the features of healthy motors as well as faulty motors is necessary. As shown in Fig. 4(b), the proposed fault detection scheme can be utilized for online usage after the development of a feature knowledge database performed in Fig. 4(a). As shown in Fig. 4, online diagnosis of motor faults comprises of three steps:

1) applying the FFT to identify the current inverter frequency from newly collected current data;
2) applying the independent components that are obtained using the training stator current data to obtain the FFT-ICA features and performing normalization;
3) detecting the motor problems according to the principle of maximum similarity by comparing its normalized FFT-ICA features with those in the feature knowledge database.

B. Data Collections and Preparations for Building the Feature Knowledge Database

The previous experimental setup [5], [6] for collecting diagnostic data from laboratory induction motors is leveraged in this research for building the feature knowledge database. The stator current waveform data are collected from both the healthy and faulty motors. Bearing and broken-rotor-bar faults as shown in Fig. 5 presented in [5] and [6] are used for the case studies in this paper.

All faulty and healthy induction motors are driven by the same voltage-fed pulse width modulated inverter. During data collection, the induction motors were each loaded with a DC generator and a variable resistance. Their stator currents are measured with a four-channel digital oscilloscope from

each of the three motors [5], [6]. Experiments are conducted with resistance increasing from zero to full load in five steps [registering six different levels: level 0 (no load), level 1, level 2, ..., level 5].

Based on the previous experiments [5], [6], the induction motors are connected to the 3-phase ac power supply through an inverter. The inverter provides a selection of variable frequency from 0 to 55 Hz. In this paper, six frequencies (20, 25, 37.5, 43.5, 50, and 55) are arbitrarily selected for the case study. The stator current waveforms are collected from each motor at each frequency at the selected sampling rate for 20 s.

It is well known that the resolution (represented as $\Delta\omega$) or the sampling rate is critical to discern the peaks and there must not be any important information missing from the measured signal data. However, greater resolution requires higher sampling rate and thus higher data storage. Initially, to meet the requirements of high resolution, a high sampling rate of 50 kHz was done using the oscilloscope with a data length of 1 M samples (=20 s × 50 kHz) over a sampling duration of 20 s. Subsequently, by progressively reducing the sample size and evaluating the resulting accuracy of the detection against the desired level, the final frequency value of 3.84 kHz is attained.

At each inverter frequencies of 20, 25, 37.5, 43.5, 50, and 55 Hz and under each load level, 30 current waveforms are collected from each kind of the motors. One-fifth of the data are used for training and four-fifth for testing.

C. Theoretical Analysis for Supporting the Proposed Scheme

The frequency-domain signatures $F(\omega)$ can be obtained from a time-domain waveform $f(t)$ by using FFT

$$f(t) \rightarrow (f(t_1) \quad f(t_2) \quad \cdots \quad f(t_L)) \tag{4}$$

$$F(\omega) = \mathrm{FFT}(f(t)) \tag{5}$$

where $f(t_i)(i = 1, 2, \ldots, L)$ represents the amplitude at time $t_i(i = 1, 2, \ldots, L)$, L is a record length of samples, and FFT represents FFT function. The frequency-domain signatures $F(\omega)$ generated by this transformation include the magnitude information about each frequency components as follows:

$$F(\omega) \rightarrow (a(\omega_1) \quad a(\omega_2) \quad \cdots \quad a(\omega_N)) \tag{6}$$

where $a(\omega_i)(i = 1, 2, \ldots, N)$ is the magnitude of frequency component $\omega_i(i = 1, 2, \ldots, N)$, $\triangle\omega = \omega_{i+1} - \omega_i$ is the resolution selected, and N is the selected number of the frequency components.

$F(\omega)$ in (6) represents the frequency-domain signatures of the healthy motor. From the stator current signals of two faulty motors, $f_{\mathrm{br}}(t)$ and $f_{\mathrm{be}}(t)$, corresponding frequency-domain signatures, $F_{\mathrm{br}}(\omega)$ and $F_{\mathrm{be}}(\omega)$, can be obtained similarly

$$F_{\mathrm{br}}(\omega) \rightarrow (a_{\mathrm{br}}(\omega_1) \quad a_{\mathrm{br}}(\omega_2) \quad \cdots \quad a_{\mathrm{br}}(\omega_N)) \tag{7}$$

$$F_{\mathrm{be}}(\omega) \rightarrow (a_{\mathrm{be}}(\omega_1) \quad a_{\mathrm{be}}(\omega_2) \quad \cdots \quad a_{\mathrm{be}}(\omega_N)) \tag{8}$$

where $a_{\mathrm{br}}(\omega_i)(i = 1, 2, \ldots, N)$ and $a_{\mathrm{be}}(\omega_i)$ $(i = 1, 2, \ldots, N)$ are the magnitudes of frequency components $\omega_i(i = 1, 2, \ldots, N)$ of broken-rotor-bar motors and bearing fault motors, respectively.

According to (1) and (2), the frequency spectrum of the broken-rotor-bar motor has sidebands around the fundamental harmonics, and the frequency spectrum of the bearing fault motor is with the frequency signatures of the bearing faults compared with that of the healthy motor. Therefore, (6)–(8) can be merged into the following:

$$F\_\text{signals} = \begin{pmatrix} a(\omega_1)\cdots a(\omega_n) & \overbrace{0\cdots 0}^{k} & \overbrace{0\cdots 0}^{m} \\ a(\omega_1)\cdots a(\omega_n) & a(\omega_{\mathrm{br1}})\cdots a(\omega_{\mathrm{brk}}) & \overbrace{0\cdots 0}^{m} \\ a(\omega_1)\cdots a(\omega_n) & \overbrace{0\cdots 0}^{k} & a(\omega_{\mathrm{be1}})\cdots a(\omega_{\mathrm{bem}}) \end{pmatrix} \tag{9}$$

where n represents the number of characteristic frequencies of the healthy motor, k represents the number of characteristic frequencies of the broken-rotor-bar motor, and m represents the number of characteristic frequencies of the bearing fault motor.

Equation (9) can be simplified as

$$F\_\text{signals} = \begin{pmatrix} A_b & 0 & 0 \\ A_b & A_{\mathrm{br}} & 0 \\ A_b & 0 & A_{\mathrm{be}} \end{pmatrix} \tag{10}$$

where $A_b = \big(a(\omega_1) \;\; a(\omega_2) \;\; \cdots \;\; a(\omega_n)\big)$ represents the frequency characteristics of the healthy motor, which are also the basic characteristics of all the motors, $A_{\mathrm{br}} = (a(\omega_{\mathrm{br1}})\; a(\omega_{\mathrm{br2}}) \;\cdots\; a(\omega_{\mathrm{brk}}))$ represents the frequency characteristics of the motor with broken-rotor-bars, and $A_{\mathrm{be}} = (a(\omega_{\mathrm{be1}})\; a(\omega_{\mathrm{be2}}) \;\cdots\; a(\omega_{\mathrm{bem}}))$ represents the frequency characteristics of bearing fault motors.

The first row of (9) and (10) represents the magnitudes of different frequency components about the healthy motor, i.e., the magnitudes of healthy motor frequency signatures. Because the healthy motor is assumed to be ideally normal, the magnitudes of faulty frequency components are zero. Similarly, the second row of (9) and (10) shows the magnitudes of frequency signatures of broken-rotor-bar motors, and the magnitudes of bearing fault frequency components are zero. The third row shows the magnitudes of frequency signatures of bearing fault motors and the magnitudes of broken-rotor-bar fault frequency components are zero, as shown in (9) and (10).

According to (9) and (10), different faults cause their frequency-domain signatures to have different frequency signatures, such as A_{br} and A_{be}. The most important observation is that frequency characteristics of healthy or faulty motors are in fact represented by the magnitudes of the frequency components rather than the frequency components themselves. This means that if the frequency components are fundamental constants, only the magnitudes of the frequency components are used to detect faults from healthy motors according to (9) and (10) regardless of other information or parameters of the motor.

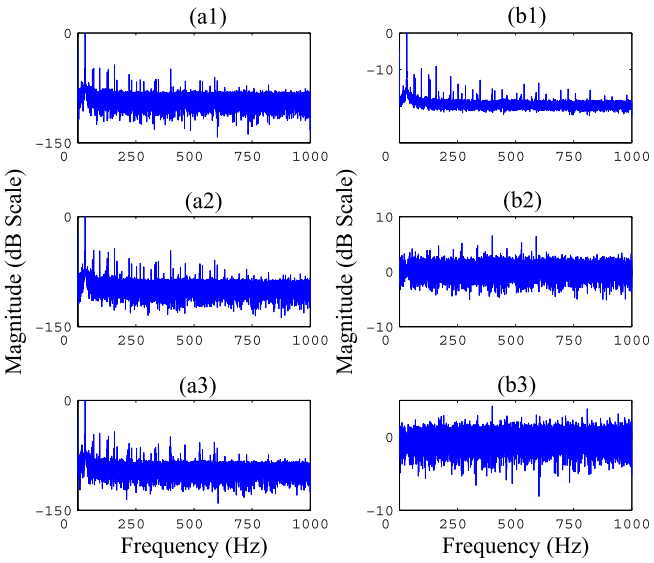

Fig. 6. FFT results in frequency domain using decibel scale and the obtained independent components from them. (a1) $F_$Signal of a healthy motor. (a2) $F_$Signal of a bearing fault motor. (a3) $F_$Signal of a motor with the broken-rotor-bar fault. (b1)–(b3) Independent components obtained from the signatures of (a1)–(a3).

According to the above theoretical analysis, only the magnitudes of the selected frequency components in (9) and (10) are used to calculate the features for the proposed fault detection scheme, as shown in Fig. 4. This allows the proposed method to overcome the challenges mentioned above.

D. FFT-ICA Feature Analysis for the Proposed Scheme

According to the ICA algorithms [33], [34], [36], [37], the frequency signatures shown in (9) and (10) can be represented as follows:

$$F\_\text{Signals} = A \cdot \text{IC}_s \tag{11}$$

where IC_s is a set of vectors that represents independent components and A is a constant matrix to be estimated. By rearranging (11), the independent components IC_s is obtained as follows [5], [6], [36], [37]:

$$\text{IC}_s = W \cdot F\_\text{Signals} \tag{12}$$

where W is the (pseudo)inverse of the matrix A of (11), which is known as the transformation matrix [5], [6], [36], [37].

Using the vectors of $F_$Signals in (9), the statistically extracted independent components, IC_s, in (12) is expressed in the form as below

$$IC_s = \begin{pmatrix} \text{IC}_1 \\ \text{IC}_2 \\ \text{IC}_3 \end{pmatrix} = \begin{pmatrix} ic11 & ic12 & \dots & ic1N \\ ic21 & ic22 & \dots & ic2N \\ ic31 & ic32 & \dots & ic3N \end{pmatrix}. \tag{13}$$

The resulting independent components IC_s reflects in the characteristic of signatures $F_$Signals in (12). Each $\text{IC}_i (i = 1, 2, \dots)$ in (13) is of the same length and in the same unit as each of the $F_$Signals [5], [6], [36], [37].

The examples of FFT results and the obtained independent components from them are shown in Fig. 6. Using (12), performing ICA on the chosen sets of the FFT results (signatures) that are shown in Fig. 6(a1)–(a3), the independent components as shown in Fig. 6(b1)–(b3) are obtained.

IC_s as well as the signatures $F_$Signals are then used to calculate FFT-ICA features as follows:

$$F\_\text{Features} = F\_\text{Signals} \cdot \text{ICs}^T \tag{14}$$

where $F_$Features are the FFT-ICA features of the frequency signatures $F_$Signals.

According to (14), the signatures, $F_$Signals, and the obtained independent components IC_s contribute to the FFT-ICA features. In other words, all the magnitude information of the frequency components in frequency signatures $F_$Signals have contributions to the FFT-ICA features. There is no need to know the exact value of the parameters, k and m, in (9) for the proposed method.

For example, F_Signal_i is the frequency-domain signatures of the i^{th} time-domain waveform

$$F\_\text{Signal}_i = (\, a_i(\omega 1) \quad a_i(\omega 2) \quad \dots \quad a_i(\omega N)\,) \tag{15}$$

where $a_i(\omega 1), a_i(\omega 2), \dots, a_i(\omega N)$ represents the magnitude information about frequency components, $\omega 1, \omega 2, \dots, \omega N$, respectively.

F_Signal_i can be converted to an M-dimension feature by independent components IC_s

$$\begin{aligned} &(F\_\text{Feature}_{i1} \quad F\_\text{Feature}_{i2} \quad \dots \quad F\_\text{Feature}_{iM}) \\ &\quad = F\_\text{Signal}_i \cdot \begin{pmatrix} ic_{11} & ic_{12} & \dots & ic_{1N} \\ ic_{21} & ic_{21} & \dots & ic_{2N} \\ \dots & \dots & \dots & \dots \\ ic_{M1} & ic_{M1} & \dots & ic_{MN} \end{pmatrix}^T \end{aligned} \tag{16}$$

where $F\_\text{Feature}_{i1}, F\_\text{Feature}_{i2}, \dots, F\_\text{Feature}_{iM}$ represent FFT-ICA feature 1, FFT-ICA feature 2, $\dots$, and FFT-ICA feature M of the i^{th} signature F_Signal_i, respectively.

A frequency-domain signature F_Signal_i from the stator current signal data is transferred to a low-dimension feature F_Feature_{i1}, $F\_\text{Feature}_{i2}, \dots, F\_\text{Feature}_{iM}$. It means that a higher dimension signature was mapped into a lower dimension feature since $M \ll N$.

As shown in (15) and (16), all the magnitude information of the selected frequency components were used to compute the M-dimension feature of the signatures. All the M-dimension features of training data from the healthy and faulty motors were exploited for establishing healthy and faulty feature database, as shown in Fig. 4(a), for fault detection of their faults, such as the broken-rotor-bar and bearing faults.

The proposed scheme estimates the value of each new inverter frequency f_s and adjusts the frequency range according to $\omega 1$ and ωN. This paper carried out the analysis using different frequency ranges. After testing the accuracy of the proposed scheme, the selected frequency range [0, 1000] is found to be good enough. Apart from achieving a high computational efficiency, the dynamically reduced frequency range also improved the noise immunity of the proposed algorithm, as noise in measurement switching transients and high-order harmonics occurs mostly at frequencies much higher than the frequency range of [0, 1000].

E. Development of Feature Knowledge Database Considering the Effect of Load and Different Inverter Frequencies

The feature knowledge database is built using the stator current waveform from the healthy and the faulty motors under each load level at each inverter frequency. Both the load and inverter frequency affect the frequency signatures of faulty motors. Therefore, (10) can be extended according to (i, j) (i represents the different inverter frequency and in order to make it easy, $i = 1, 2, \ldots, I$ level is used in this paper and j represents the load level, and in this paper, $j = 1, 2, \ldots, L$)

$$F\_\text{signals} = \begin{pmatrix} A_b(1,1) & 0 & 0 \\ A_b(1,1) & A_{\text{br}}(1,1) & 0 \\ A_b(1,1) & 0 & A_{\text{be}}(1,1) \\ \\ A_b(1,2) & 0 & 0 \\ A_b(1,2) & A_{\text{br}}(1,2) & 0 \\ A_b(1,2) & 0 & A_{\text{be}}(1,2) \\ \vdots & \vdots & \vdots \\ A_b(1,L) & 0 & 0 \\ A_b(1,L) & A_{\text{br}}(1,L) & 0 \\ A_b(1,L) & 0 & A_{\text{be}}(1,L) \\ \vdots & \vdots & \vdots \\ A_b(I,L) & 0 & 0 \\ A_b(I,L) & A_{\text{br}}(I,L) & 0 \\ A_b(I,L) & 0 & A_{\text{be}}(I,L) \end{pmatrix} \tag{17}$$

where in each element $A_T(i, j)$, T represents the type of motor (b: healthy, br: broken-rotor-bar fault, and be: bearing fault), in which i represents the supply frequency level and j represents the load level. All those data are used to establish the database of Fig. 4(a).

Equation (17) can be rearranged as

$$F\_\text{signals} = \begin{pmatrix} A_b(1,1) & 0 & 0 \\ A_b(1,2) & 0 & 0 \\ \vdots & \vdots & \vdots \\ A_b(I,L) & 0 & 0 \\ A_b(1,1) & A_{\text{br}}(1,1) & 0 \\ A_b(1,2) & A_{\text{br}}(1,2) & 0 \\ \vdots & \vdots & \vdots \\ A_b(I,L) & A_{\text{br}}(I,L) & 0 \\ A_b(1,1) & 0 & A_{\text{be}}(1,1) \\ A_b(1,2) & 0 & A_{\text{be}}(1,2) \\ \vdots & \vdots & \vdots \\ A_b(I,L) & 0 & A_{\text{be}}(I,L) \end{pmatrix} \tag{18}$$

where

$$F\_\text{signals}\_A_b(i,j) = \begin{pmatrix} A_b(i,j) & 0 & 0 \end{pmatrix} \tag{19}$$

represents the signatures of healthy motors, which are the benchmarks of

$$F\_\text{signals}\_A_{\text{br}}(i,j) = \begin{pmatrix} A_b(i,j) & A_{\text{br}}(i,j) & 0 \end{pmatrix} \tag{20}$$

and

$$F\_\text{signals}\_A_{\text{be}}(i,j) = \begin{pmatrix} A_b(i,j) & 0 & A_{\text{be}}(i,j) \end{pmatrix}. \tag{21}$$

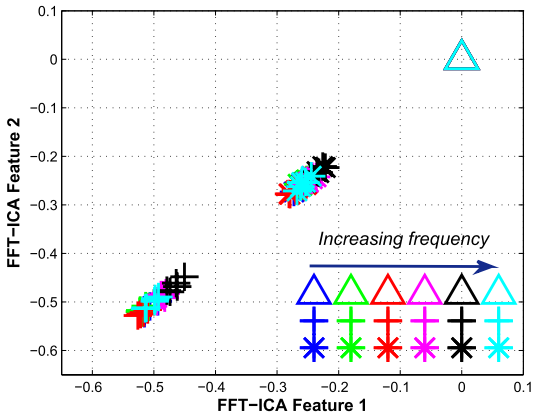

Fig. 7. Simulation results of the proposed scheme. Δ's—healthy. +'s—bearing fault. ∗'s—broken-rotor-bar fault. Blue Δ's, +'s, and ∗'s—20 Hz. Green Δ's, +'s, and ∗'s—25 Hz. Red Δ's, +'s, and ∗'s—37.5 Hz. Pink Δ's, +'s, and ∗'s—43.5 Hz. Black Δ's, +'s, and ∗'s—50 Hz. Cyan Δ's, +'s, and ∗'s—55 Hz.

As mentioned in Section IV-B, stator current data are collected from the healthy and faulty motors running at six inverter frequencies, under no load and five other load levels (six load levels in this paper), respectively. To provide a holistic view of the healthy and faulty motors' feature knowledge database, each FFT-ICA feature, which is obtained using (16), is normalized using the corresponding FFT-ICA feature of the healthy motor as a benchmark to form the feature knowledge database. After establishing the feature knowledge database, each newly measured set of stator current data is imputed into the second module as shown in Fig. 4(b) for performing fault detection.

V. Simulation Results and Performance of the Proposed Scheme for the Case Study

The proposed scheme is validated in the laboratory using three-phase, two-pole, 1.1 kW induction motors. The motors are supplied with different frequencies: 20, 25, 37.5, 43.5, 50, and 55 Hz. For each induction motor case, 30 current signal segments are collected from each motor at each frequency. The statistical analysis carried out to detect fault is described next.

A. Two Broken Rotor Bars and Bearing Fault

Fig. 7 shows the simulation results of the proposed scheme. Both the training and testing results are almost similar to each other to the point where they overlap. Compared with the time-domain algorithm (Figs. 2 and 3), the proposed algorithm outperforms the previous algorithm and there is no drift (Fig. 3) in the two faulty clusters with changing inverter frequency, as shown in Fig. 7. This demonstrates robustness and reliability of the proposed method.

Fig. 8(a) and (b) shows the normalized FFT-ICA features versus inverter frequency. More importantly, the dimensionality reduction of the new FFT-ICA feature space is observed. The FFT-ICA features have the same discriminative power, which implies that for the problems in this paper, only one FFT-ICA feature will be adequate for classifying the fault motors from healthy motors across all inverter frequencies.

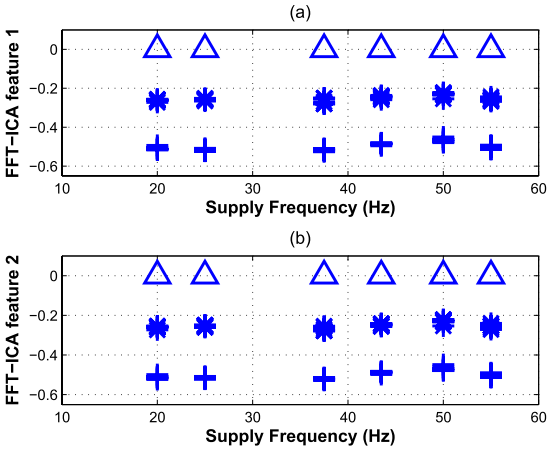

Fig. 8. Two FFT-ICA features versus inverter frequency after normalization using healthy motors as the benchmarks.

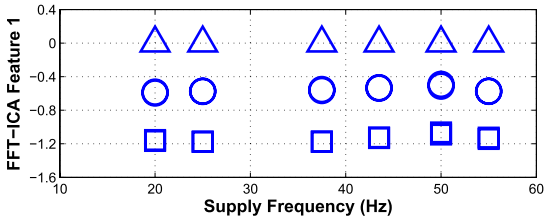

Fig. 9. Simulation results of the FFT-ICA feature 1; Δ's—healthy motor. ○'s—one-broken-rotor-bar motor. □'s—half-broken-rotor-bar motor.

B. One Broken Rotor Bar and Half Broken Rotor Bar

The normalized FFT-ICA features for healthy, half-broken-rotor-bar, and one-broken-rotor-bar motors are compared with those in the knowledge database in Fig. 9 and are shown to match very well. In this paper, the magnitudes of the fault frequencies are used to detect faults from induction motors. However, the difference between the detection of half-broken-rotor-bar, one-broken-rotor-bar fault, and two-broken-rotor-bar fault is just in the magnitude of the feature frequencies [38]. In addition, according to the theoretical spectrum analysis, the spectral lines of the feature frequencies of the half-broken-rotor-bar and one-broken-rotor-bar faults are slightly less than that of the two-broken-rotor-bar fault [39], [40]. Therefore, for the same motor at certain inverter-frequency and under certain load level, the spectral lines of the feature frequencies of the half-broken-rotor-bar, one-broken-rotor-bar, and two-broken-rotor-bar faults are unique [23], [38], [39], [41]. The ICA has been demonstrated to be capable of capturing the healthy and faulty independent components. This means that the proposed scheme can distinctly differentiate the half-broken-rotor-bar and one-broken-rotor-bar faults of the motor according to the spectral lines of the feature frequencies. On the other hand, the challenges for detecting half-broken-rotor-bar and one-broken-rotor-bar faults are also encountered in detecting the two-broken-rotor-bar fault of induction motors. Under no-load condition, it is difficult to separate the feature frequencies f_{bL} and f_{bR} of the broken-rotor-bar motor from f_s because they are very closely located in the frequency spectrum [21], [38]. The proposed scheme that detects the two-broken-rotor-bar fault in this paper can also effectively address the challenges of detection of half-broken-rotor-bar and one-broken-rotor-bar faults. Based on the above analysis, as long as the feature knowledge database contains feature components of half-broken-rotor-bar fault, one-broken-rotor-bar fault, and other faults, the proposed scheme is able to detect the actual fault type of induction motors.

TABLE I

COMPARISON BETWEEN THE PROPOSED METHODOLOGY AND THE PREVIOUS METHODOLOGY

Motor Condition	Accuracy	Ref. [28]	Ref. [29]
Broken rotor bar, 20 Hz	100%	90%	98%
Broken rotor bar, 25 Hz	100%	95%	99%
Broken rotor bar, 37.5 Hz	100%	100%	100%
Broken rotor bar, 43.5 Hz	100%	100%	100%
Broken rotor bar, 50 Hz	100%	100%	100%
Broken rotor bar, 55 Hz	100%	100%	100%

As mentioned in Section IV-B, one-fifth of data were used for training and four-fifth have been used for testing. According to the simulation results, all 1080 samples (360 healthy, 360 bearing faults and 360 broken-rotor-bars or 360 half-broken-rotor-bars and 360 one-broken-rotor-bars) were classified correctly. Both classification for rate the training and testing accuracy achieved 100% for the problem in this paper.

As discussed in Sections I and II, many existing frequency-based techniques require the user to possess some level of expertise regarding the motor parameters, operations, and design that are all dependent information on motors. These collectively make online applications difficult.

The scheme proposed in this paper provides a solution that overcomes the challenges mentioned above. Using the proposed scheme, one only needs to input a new set of motor current signal data, as the fault feature database is already established. The ensuing online fault detection can then be fully automated. Thus, the proposed feature knowledge based fault detection scheme is an ideal potential procedure for online monitoring of induction motors, especially in remote locations, where manual inspections are expensive or even unavailable. Due to its simplicity, the proposed algorithm is ideal also for implementation on the fault detection of other pieces of equipment, as the majority of computation involves simple data processing of the features of the obtained data and estimation of the new data as input for the proposed method.

The computation of the FFT-ICA features of a new stator current waveform involves only simple partial substitution of the obtained FFT results into (16) in ICA Block B as shown in Fig. 4. The comparison block simply requires retrieval of data from the fault signature database, and normalizing and comparing the newly computed FFT-ICA feature against preset levels. The comparisons of the previous methods, such as time-domain methods, frequency-domain methods, hybrid time–frequency-domain analysis algorithms, and park transform with the MFN method [14], [15], [28], [29], with the method implemented in this paper is shown in Table I. The proposed scheme has shown to give better results under changing frequency. Because this paper leverages on the magnitude of the stator current frequency components and the frequency components for both the healthy and faulty motors,

it has shown that the conditions with broken-rotor-bar and bearing faults can now be more accurately diagnosed.

VI. Conclusion

This paper has presented a new scheme for online fault detection in induction motors that makes use of a newly created healthy and faulty feature knowledge database, making the method highly scalable. The first stage of the proposed scheme relies on analyzing the training stator current signals. In this paper, the magnitudes of the stator current frequency components represent the frequency characteristics of healthy or faulty motors by theoretical analysis. Both FFT and ICA methods are applied in this stage in order to extract independent components. The resultant independent components and the obtained frequency signatures are both used to calculate the features, which are referred to as FFT-ICA features. The FFT-ICA features were further analyzed to form a feature knowledge database. In the second stage, for the online monitoring of the stator current data, FFT and ICA were utilized to calculate the FFT-ICA features, which were normalized accordingly to build a feature knowledge database. Finally, the similarity principle is applied to identify the fault type. The simulation results of broken-rotor-bar and bearing faults at each inverter frequencies of 20, 25, 37.5, 43.5, 50, and 55 Hz and under each load level were proven to be highly efficient in bringing about a diagnosis of the induction motor of the proposed scheme. In addition, the proposed scheme could improve the efficiency of online detection at each inverter frequency and under each load level after finishing the offline training.

There are some important issues that are not studied in this paper. First, this paper investigates motor fault detection by only focusing on two main faults. Other fault types should also be investigated, and especially building a feature knowledge database for motors with more than one fault should be considered. Second, while the faults can be differentiated correctly from the healthy motors, the severity of the faults is not investigated in this paper. Therefore, studies to incorporate the severity of the faults are needed for future work.

Acknowledgment

The authors would like to thank the researchers and experts from Rolls-Royce for the valuable discussions. The authors would also like to thank other team members of the Institute of High Performance Computing, A*STAR, and researchers and experts from the National University of Singapore for their assistance and essential help in conducting this study.

References

[1] J. Antonino-Daviu, S. Aviyente, E. G. Strangas, and M. Riera-Guasp, "Scale invariant feature extraction algorithm for the automatic diagnosis of rotor asymmetries in induction motors," *IEEE Trans. Ind. Informat.*, vol. 9, no. 1, pp. 100–108, Feb. 2013.

[2] Y.-H. Kim, Y.-W. Youn, D.-H. Hwang, J.-H. Sun, and D.-S. Kang, "High-resolution parameter estimation method to identify broken rotor bar faults in induction motors," *IEEE Trans. Ind. Electron.*, vol. 60, no. 9, pp. 4103–4117, Sep. 2013.

[3] L. M. Contreras-Medina, R. de Jesus Romero-Troncoso, E. Cabal-Yepez, J. de Jesus Rangel-Magdaleno, and J. R. Millan-Almaraz, "FPGA-based multiple-channel vibration analyzer for industrial applications in induction motor failure detection," *IEEE Trans. Instrum. Meas.*, vol. 59, no. 1, pp. 63–72, Jan. 2010.

[4] S. X. Ding, P. Zhang, S. Yin, and E. L. Ding, "An integrated design framework of fault-tolerant wireless networked control systems for industrial automatic control applications," *IEEE Trans. Ind. Informat.*, vol. 9, no. 1, pp. 462–471, Feb. 2013.

[5] Z. Wang and C. S. Chang, "Online fault detection of induction motors using frequency domain independent components analysis," in *Proc. IEEE Int. Symp. Ind. Electron. (ISIE)*, Jun. 2011, pp. 2132–2137.

[6] Z. Wang, C. S. Chang, and Y. Zhang, "A feature based frequency domain analysis algorithm for fault detection of induction motors," in *Proc. 6th IEEE Conf. Ind. Electron. Appl. (ICIEA)*, Jun. 2011, pp. 27–32.

[7] M. Shahbazi, P. Poure, S. Saadate, and M. R. Zolghadri, "FPGA-based fast detection with reduced sensor count for a fault-tolerant three-phase converter," *IEEE Trans. Ind. Informat.*, vol. 9, no. 3, pp. 1343–1350, Aug. 2013.

[8] A. Singhal and M. A. Khandekar, "Bearing fault detection in induction motor using fast Fourier transform," in *Proc. IEEE Int. Conf. Adv. Res. Eng. Technol.*, Feb. 2013, pp. 190–194.

[9] A. Soualhi, G. Clerc, and H. Razik, "Detection and diagnosis of faults in induction motor using an improved artificial ant clustering technique," *IEEE Trans. Ind. Electron.*, vol. 60, no. 9, pp. 4053–4062, Sep. 2013.

[10] F. Immovilli, C. Bianchini, M. Cocconcelli, A. Bellini, and R. Rubini, "Bearing fault model for induction motor with externally induced vibration," *IEEE Trans. Ind. Electron.*, vol. 60, no. 8, pp. 3408–3418, Aug. 2013.

[11] X. Dai and Z. Gao, "From model, signal to knowledge: A data-driven perspective of fault detection and diagnosis," *IEEE Trans. Ind. Informat.*, vol. 9, no. 4, pp. 2226–2238, Nov. 2013.

[12] X. Jin and T. W. S. Chow, "Anomaly detection of cooling fan and fault classification of induction motor using Mahalanobis–Taguchi system," *Expert Syst. Appl.*, vol. 40, no. 15, pp. 5787–5795, 2013.

[13] A. Sadeghian, Z. Ye, and B. Wu, "Online detection of broken rotor bars in induction motors by wavelet packet decomposition and artificial neural networks," *IEEE Trans. Instrum. Meas.*, vol. 58, no. 7, pp. 2253–2263, Jul. 2009.

[14] Z.-X. Wang, C. S. Chang, X. German, and W. W. Tan, "Online fault detection of induction motors using independent component analysis and fuzzy neural network," in *Proc. 8th IET Int. Conf. Adv. Power Syst. Control, Oper. Manage.*, Hong Kong, 2009, p. 321.

[15] T. W. Chua, W. W. Tan, Z.-X. Wang, and C. S. Chang, "Hybrid time-frequency domain analysis for inverter-fed induction motor fault detection," in *Proc. IEEE Int. Symp. Ind. Electron. (ISIE)*, Jul. 2010, pp. 1633–1638.

[16] M. Seera, C. P. Lim, S. Nahavandi, and C. K. Loo, "Condition monitoring of induction motors: A review and an application of an ensemble of hybrid intelligent models," *Expert Syst. Appl.*, vol. 41, no. 10, pp. 4891–4903, 2014.

[17] M. Drif and A. J. M. Cardoso, "Stator fault diagnostics in squirrel cage three-phase induction motor drives using the instantaneous active and reactive power signature analyses," *IEEE Trans. Ind. Informat.*, vol. 10, no. 2, pp. 1348–1360, May 2014.

[18] E. H. El Bouchikhi, V. Choqueuse, and M. Benbouzid, "Induction machine faults detection using stator current parametric spectral estimation," *Mech. Syst. Signal Process.*, vols. 52–53, pp. 447–464, Feb. 2015.

[19] J. Faiz, V. Ghorbanian, and B. M. Ebrahimi, "EMD-based analysis of industrial induction motors with broken rotor bars for identification of operating point at different supply modes," *IEEE Trans. Ind. Informat.*, vol. 10, no. 2, pp. 957–966, May 2014.

[20] A. M. da Silva, R. J. Povinelli, and N. A. O. Demerdash, "Rotor bar fault monitoring method based on analysis of air-gap torques of induction motors," *IEEE Trans. Ind. Informat.*, vol. 9, no. 4, pp. 2274–2283, Nov. 2013.

[21] M. Fernandez-Temprano, P. E. Gardel-Sotomayor, O. Duque-Perez, and D. Morinigo-Sotelo, "Broken bar condition monitoring of an induction motor under different supplies using a linear discriminant analysis," in *Proc. 9th IEEE Int. Symp. Diagnostics Electr. Mach., Power Electron. Drives (SDEMPED)*, Aug. 2013, pp. 162–168.

[22] J. Seshadrinath, B. Singh, and B. K. Panigrahi, "Investigation of vibration signatures for multiple fault diagnosis in variable frequency drives using complex wavelets," *IEEE Trans. Power Electron.*, vol. 29, no. 2, pp. 936–945, Feb. 2014.

[23] J. de Jesus Rangel-Magdaleno, H. Peregrina-Barreto, J. M. Ramirez-Cortes, P. Gomez-Gil, and R. Morales-Caporal, "FPGA-based broken bars detection on induction motors under different load using motor current signature analysis and mathematical morphology," *IEEE Trans. Instrum. Meas.*, vol. 63, no. 5, pp. 1032–1040, May 2014.

[24] W. S. Gongora, H. V. D. Silva, A. Goedtel, W. F. Godoy, and S. A. Q. da Silva, "Neural approach for bearing fault detection in three phase induction motors," in *Proc. 9th IEEE Int. Symp. Diagnostics Electr. Mach., Power Electron. Drives (SDEMPED)*, Aug. 2013, pp. 566–572.
[25] O. Duque-Perez, L.-A. Garcia-Escudero, D. Morinigo-Sotelo, P.-E. Gardel, and M. Perez-Alonso, "Analysis of fault signatures for the diagnosis of induction motors fed by voltage source inverters using ANOVA and additive models," *Electr. Power Syst. Res.*, vol. 121, pp. 1–13, Apr. 2015.
[26] M. Sahraoui, A. Ghoggal, S. E. Zouzou, and S. Guedidi, "Rotor fault detection algorithm based on a new fault indicator for induction motors fed from an industrial frequency inverter," *Int. J. Appl. Electromagn. Mech.*, vol. 47, no. 2, pp. 483–502, 2015.
[27] O. Duque-Perez, L. A. Garcia-Escudero, D. Morinigo-Sotelo, P. E. Gardel, and M. Perez-Alonso, "Condition monitoring of induction motors fed by voltage source inverters. Statistical analysis of spectral data," in *Proc. 20th Int. Conf. Elect. Mach. (ICEM)*, Sep. 2012, pp. 2479–2484.
[28] A. G. Garcia-Ramirez, R. A. Osornio-Rios, D. Granados-Lieberman, A. Garcia-Perez, and R. J. Romero-Troncoso, "Smart sensor for online detection of multiple-combined faults in VSD-fed induction motors," *Sensors*, vol. 12, no. 9, pp. 11989–12005, 2012.
[29] A. G. Garcia-Ramirez, R. A. Osornio-Rios, A. Garcia-Perez, and R. J. Romero-Troncoso, "FPGA-based smart-sensor for fault detection in VSD-fed induction motors," in *Proc. 9th IEEE Int. Symp. Diagnostics Electr. Mach., Power Electron. Drives (SDEMPED)*, Aug. 2013, pp. 233–240.
[30] M. J. Picazo-Ródenas, J. Antonino-Daviu, V. Climente-Alarcon, R. Royo-Pastor, and A. Mota-Villar, "Combination of noninvasive approaches for general assessment of induction motors," *IEEE Trans. Ind. Appl.*, vol. 51, no. 3, pp. 2172–2180, May/Jun. 2015.
[31] S. Toscani, M. Faifer, M. Rossi, L. Cristaldi, and M. Lazzaroni, "Effects of the speed loop on the diagnosis of rotor faults in induction machines," *IEEE Trans. Instrum. Meas.*, vol. 61, no. 10, pp. 2713–2722, Oct. 2012.
[32] J.-H. Jung, J.-J. Lee, and B.-H. Kwon, "Online diagnosis of induction motors using MCSA," *IEEE Trans. Ind. Electron.*, vol. 53, no. 6, pp. 1842–1852, Dec. 2006.
[33] X. Ma, H. Zhang, X. Zhao, L. Yao, and Z. Long, "Semi-blind independent component analysis of fMRI based on real-time fMRI system," *IEEE Trans. Neural Syst. Rehabil. Eng.*, vol. 21, no. 3, pp. 416–426, May 2013.
[34] M. A. M. Ariff and B. C. Pal, "Coherency identification in interconnected power system—An independent component analysis approach," *IEEE Trans. Power Syst.*, vol. 28, no. 2, pp. 1747–1755, May 2013.
[35] A. Widodo, B.-S. Yang, and T. Han, "Combination of independent component analysis and support vector machines for intelligent faults diagnosis of induction motors," *Expert Syst. Appl.*, vol. 32, no. 2, pp. 299–312, 2007.
[36] M. Razavian, M. H. Hosseini, and R. Safian, "Time-reversal imaging using one transmitting antenna based on independent component analysis," *IEEE Geosci. Remote Sens. Lett.*, vol. 11, no. 9, pp. 1574–1578, Sep. 2014.
[37] H. Mehrabian, R. Chopra, and A. L. Martel, "Calculation of intravascular signal in dynamic contrast enhanced-MRI using adaptive complex independent component analysis," *IEEE Trans. Med. Imag.*, vol. 32, no. 4, pp. 699–710, Apr. 2013.
[38] J. de Jesus Rangel-Magdaleno, R. de Jesus Romero-Troncoso, R. A. Osornio-Rios, E. Cabal-Yepez, and L. M. Contreras-Medina, "Novel methodology for online half-broken-bar detection on induction motors," *IEEE Trans. Instrum. Meas.*, vol. 58, no. 5, pp. 1690–1698, May 2009.
[39] A. Garcia-Perez, R. J. Romero-Troncoso, E. Cabal-Yepez, R. A. Osornio-Rios, J. de Jesus Rangel-Magdaleno, and H. Miranda, "Startup current analysis of incipient broken rotor bar in induction motors using high-resolution spectral analysis," in *Proc. IEEE Int. Symp. Diagnostics Electr. Mach., Power Electron. Drives (SDEMPED)*, Sep. 2011, pp. 657–663.
[40] C. Pezzani, P. Donolo, G. Bossio, M. Donolo, A. Guzman, and S. E. Zocholl, "Detecting broken rotor bars with zero-setting protection," *IEEE Trans. Ind. Appl.*, vol. 50, no. 2, pp. 1373–1384, Mar./Apr. 2014.
[41] J. Martinez, A. Belahcen, and A. Arkkio, "Broken bar indicators for cage induction motors and their relationship with the number of consecutive broken bars," *IET Electr. Power Appl.*, vol. 7, no. 8, pp. 633–642, Sep. 2013.

Ting Yang is currently a Professor of Electrical Engineering with Tianjin University, Tianjin, China. He has authored or co-authored four books and over 80 publications in technical journals and conferences. His current research interests include machinery condition monitoring and diagnosis, communication, intelligent control, and data mining and processing.

Prof. Yang is a member of the International Society for Industry and Applied Mathematics, a Senior Member of the Chinese Institute of Electronic, and the Committee Member of electronic circuit and system. He is the winner of the Education Ministry's New Century Excellent Talents Supporting Plan. He has been the Chairman of two workshops of the IEEE International Conference.

Haibo Pen received the B.S. degree in electrical engineering from the China University of Mining and Technology, Xuzhou, China, in 2011. He is currently pursuing the Ph.D. degree with the School of Electrical Engineering and Automation, Tianjin University, Tianjin, China.

His current research interests include big data analytics, data mining, and fault diagnosis.

Zhaoxia Wang (M'13) received the Ph.D. degree from Nankai University, Tianjin, China.

She spent two years of post-doctoral research with Tianjin University, Tianjin. She became an Associate Professor with the School of Electronic and Information Engineering, Tianjin University of Technology, Tianjin, in 2004. She was a Research Staff Member with the Department of Electrical and Computer Engineering, National University of Singapore, Singapore, from 2008 to 2011. As an Expert in data analytics, intelligent systems, pattern recognition, and data mining, she has led and successfully delivered more than ten projects. She is currently the Principal Investigator and Research Leader of the projects relevant to big data analytics. She is a Scientist and Program Manager with the Social and Cognitive Computing Department, Institute of High Performance Computing, Agency for Science, Technology and Research, Singapore. She is an Adjunct Professor with Tianjin University. Her current research interests include soft computing, intelligent algorithms and their applications, fuzzy theory and control, fault detection and diagnosis, text mining, and social media analytics.

Prof. Wang has been an Associate Editor of *Electronic Commerce Research and Applications (ECRA)* journal since 2013.

Che Sau Chang received the Higher Diploma degree in electrical engineering from Hong Kong Polytechnic University, Hong Kong, the Diploma degree in electrical engineering from the Institution of Electrical Engineers, the M.Sc. and Ph.D. degrees from the University of Manchester Institute of Science and Technology, Manchester, U.K., and the D.Sc. degree from the University of Manchester Institute of Science and Technology, Manchester, U.K., in 2001, for achieving outstanding publishing records in his research areas.

He was with the Department of Electrical and Computer Engineering, National University of Singapore, Singapore, where he is currently with the Centre of Maritime Studies. He completed several industrial research contracts in the U.K., Hong Kong, and Singapore in the areas of railway, energy, and maritime systems. He has supervised over 50 graduate and post-doctoral student projects. He has authored or co-authored over 350 publications in international refereed journals/conference proceedings/research monographs. His current research interests include the modeling, analysis, and AI applications in railway, energy, and maritime systems.

Prof. Chang was the Technical Chair of the 2000 IEEE Winter Power Meeting in Singapore.